Available online at www.sciencedirect.com

SCIENCE DIRECT®

Earth and Planetary Science Letters 224 (2004) 337–346

EPSL

www.elsevier.com/locate/epsl

Seismic constraints on the depth and composition of the mantle keel beneath the Kaapvaal craton

Fenglin Niu[a,*], Alan Levander[a], Catherine M. Cooper[a], Cin-Ty Aeolus Lee[a], Adrian Lenardic[a], David E. James[b]

[a] *Department of Earth Science, MS-126, Rice University, 6100 Main St., Houston, TX 77005, USA*
[b] *Department of Terrestrial Magnetism, Carnegie Institution of Washington, 5241 Broad Branch Road, N.W., Washington, DC 20015, USA*

Received 28 January 2004; received in revised form 29 April 2004; accepted 10 May 2004
Available online 19 July 2004

Abstract

S–P travel-time residuals and receiver-function images are used to infer the V_p/V_s (compressional to shear wave velocity) ratio of the lithospheric mantle beneath southern African and the topography of the underlying 410-km discontinuity. Low V_p/V_s ratios provide evidence independent of geochemical observations for a highly depleted root (Mg# ~92–94) beneath the Kaapvaal craton. The receiver-function images, on the other hand, consistently show a flat 410-km discontinuity beneath the entire array. This observation, after combined with the results of geodynamical modeling, allows us to place limits on the thickness of this chemical boundary layer, which is between ~160 and ~370 km.

Keywords: S–P travel-time residual; V_p/V_s ratio; receiver-function imaging; 410-km discontinuity; Mg#; chemical boundary layer; thermal sublayer

1. Introduction

Although the existence of a thick, cold, highly depleted lithosphere—the so-called tectosphere [1,2]—beneath Archean cratons is generally accepted, its exact thickness is still controversial [3–10]. Part of the controversy is caused by the poor depth resolution in seismic tomography. An alternative seismic approach for placing limits on lithospheric thickness is by looking at the topography of the 410-km discontinuity because the thermal effects of a thick keel should result in an elevated discontinuity [11]. For example, Li et al. [12] observed a flat 410-km discontinuity beneath the eastern margin of the North American continent and concluded that mantle downwellings associated with the cold cratonic keel must be confined within the mantle above the transition zone. However, because Li et al.'s [12] study was situated on the margin of the North American continent, the topography of the 410-km discontinuity directly beneath cratonic keels has still not been investigated using data from dense seismic arrays that extend from mobile belts to craton centers. It is also important to recognize that the evidence for depleted lithospheric mantle keels un-

* Corresponding author. Department of Earth Science, MS-126, Rice University, 6100 Main St., Houston, TX 77005, USA. Tel.: +1-713-348-4122; fax: +1-713-348-5214.
E-mail address: niu@rice.edu (F. Niu).

0012-821X/$ - see front matter © 2004 Elsevier B.V. All rights reserved.
doi:10.1016/j.epsl.2004.05.011

derlying cratons is so far based largely on geochemical studies [13] of mantle xenoliths from kimberlite intrusions and not from seismic studies because the effects of temperature and composition on seismic velocities are difficult to separate. Here, we use S–P travel-time residuals and receiver-function imaging to estimate the V_p/V_s structure of the Kaapvaal cratonic keel in South Africa and the topography of the underlying 410-km discontinuity. In particular, we make use of a recent study suggesting that V_p/V_s may be more sensitive to composition [Mg# = Mg/(Mg + Fe) × 100] than temperature [14]. Collectively, this approach should allow us to constrain the composition of the mantle keel and place limits on its thickness.

Southern Africa was chosen because it is a "type locale" and because of the availability of high-quality densely sampled broadband seismic data. The crust in the Archean Kaapvaal craton in southern Africa formed between 2.6 and 3.6 Ga [15]. It is bounded on the southwest and northeast by the Proterozoic Namaqua-Natal and the Archean Limpopo belts, respectively (Fig. 1). The craton itself was subsequently modified by the large Bushveld magmatic event at ~2.05 Ga. Tomographic images of both P- and S-wave velocities [16] obtained during a recent regional seismic experiment show higher velocities (up to 1.0% in P wave and 1.5% in S wave) beneath the Kaapvaal craton relative to adjacent mobile belts. These velocity contrasts extend to depths as great as 300 km, which suggests that a deep mantle root lies beneath the Kaapvaal craton [16]. These tomographic studies therefore show that the mantle structure beneath southern Africa is correlated with geologic provinces. There also appears to be a correlation between geologic provinces and crustal structure. That

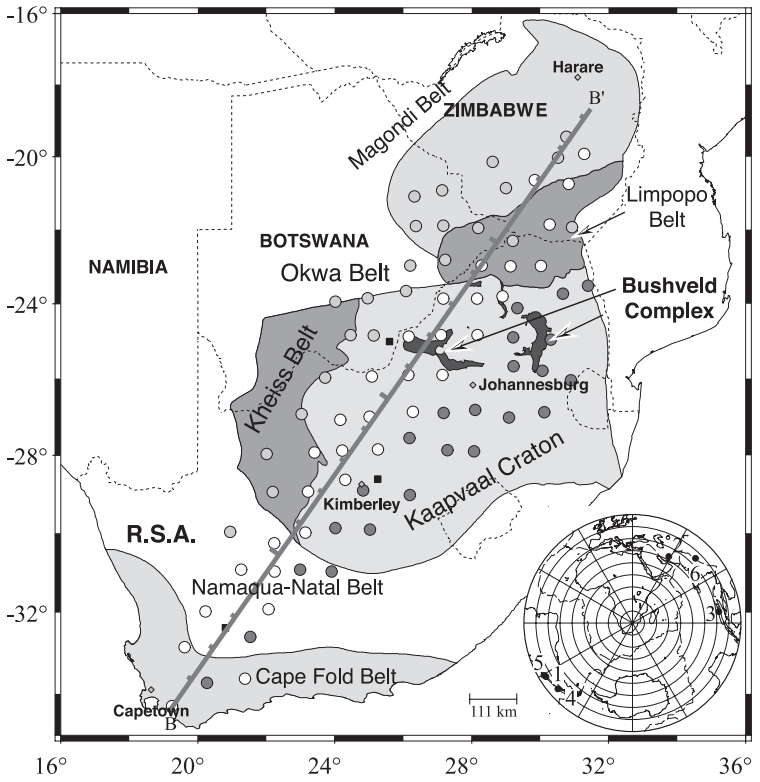

Fig. 1. Map showing the principal geologic provinces in southern Africa, and the 82 station locations (circles) of the Southern Africa Seismic Experiment. Black squares denote global digital seismic stations. Line BB′ indicates the location of the profile shown in Figs. 2 and 3, which is similar to the cross-section of Fig. 2 in [16]. Inset shows the six earthquakes used in the receiver-function imaging.

is, a thin crust and sharp crust–mantle transition is observed beneath the undisturbed Kaapvaal craton, while a thick crust and a diffuse Moho boundary is found beneath the region of the Bushveld Complex disturbance and the Proterozoic belts [17–20].

2. Data selection and analyses

The data for this study were recorded by the South Africa Seismic Experiment of the Kaapvaal Project [21]. A total of 54 broadband seismographs were deployed at 82 sites in South Africa, Zimbabwe and Botswana between April 1997 and 1999 (Fig. 1). The seismic array forms an elongated swath that extends southwest to northeast across the Archean Kaapvaal craton and adjacent Proterozoic mobile belts. Hundreds of teleseismic events were recorded by the seismic arrays. We have examined thousands of seismograms from 231 earthquakes with magnitude Mw ≥ 5.5 and at epicentral distances of 30–90°, from which we have chosen six shallow earthquakes with high signal-to-noise ratio and located roughly along the array azimuth for analysis. Source parameters of the six events are listed in Table 1.

The radial component of the teleseismic P coda is comprised in part of P to S converted waves generated at structures beneath the recording station. The structures are thus imageable through back-projecting the P coda. We employed the receiver-function technique [22,23] in the imaging. Receiver functions are commonly formed by a simple deconvolution of vertical components from radial components of teleseismic recordings. We found that a similar deconvolution between the two principle directions of P- and SV-wave [24,25] provides a slightly better means to reduce the crust reverberation. Deconvolution is performed in the frequency domain:

$$H(\omega) = \frac{P^*(\omega)}{\max\{P(\omega)P^*(\omega),\ k|P_{\max}(\omega_0)|^2\}} e^{-\left(\frac{\omega}{2a}\right)^2} \quad (1)$$

Here k is a constant known as the "water level" [26,27]. $P(\omega)$ and $V(\omega)$ are the spectra taken from a 105 s time window (5 s before and 100 s after the P) with a cosine taper of 5 s. The width factor, a, of the Gaussian lower-pass filter was set to 1 to ensure constructive stacking. The requirement for constructive stacking is $\omega \cdot \delta t < 1$, where δt is the variance of the S–P differential travel-time residuals resulting from unmodeled lateral heterogeneities. The average δt is ~0.84 s (Table 1), suggesting signals with periods longer than 5.3 s are most useful for constructive stacking.

A revised common-conversion-point stacking technique [28] was employed to enhance the signal-to-noise ratio. Following Niu et al. [29], we varied the bin size and fixed the number N of conversion points in each bin to improve the horizontal resolution in densely sampled regions. The value for N in a given bin, 10–20 depending on the signal-to-noise ratio of seismograms, was chosen so that conversions for the 410- and 660-km discontinuities were clearly visible. The bin size varies between 1° and 2° with an average of ~1.4°. For a conversion depth d, we first calculated the ray path of converted phase Pds and its arrival time relative to P by ray tracing the 1D *iasp91* velocity model [30]. We then summed the N seismograms and further averaged the summations within a 0.5 s window centered on the arrival time of Pds using an nth-root stacking method [31,32]. We chose $n = 4$

Table 1
Event list

Event no.	Origin time (mm/dd/yy min:s)	Latitude (°N)	Longitude (°E)	Depth (km)	Mw	S–P (s)
1	01/12/98 10:14	−30.985	−71.410	35.0	6.6	−1.97 ± 1.19
2	03/14/98 19:40	30.154	57.605	9.0	6.6	−1.97 ± 0.95
3	04/01/98 17:56	−0.544	99.261	56.0	7.0	0.09 ± 0.78
4	04/01/98 22:42	−40.316	−74.874	9.0	6.7	−1.83 ± 0.92
5	09/03/98 17:37	−29.450	−71.715	27.0	6.6	−1.62 ± 0.83
6	03/28/99 19:05	30.512	79.403	15.0	6.6	−3.57 ± 0.80
7[a]	10/05/97 18:04	−59.739	−29.198	274.0	6.3	−1.80 ± 0.40

[a] Is an intermediate earthquake and thus not used in receiver-function imaging.

to reduce the uncorrelated noise relative to the usual linear stack ($n=1$). We varied d from 0 to 1000 km in increments of 1 km.

3. Results and discussions

A cross section of the CCP stacked image is shown in Fig. 2A. The apparent depths of the two discontinuities defining the mantle transition zone are ~394 and 638 km, respectively. These values are consistent with previous observations in the same region [33], but are ~20 km shallower than the global averages [34,35]. This discrepancy is probably due to an inappropriate 1D reference model used in calculating the travel times. While an accurate reference model is always important in receiver-function imaging, high-resolution regional tomographic models don't necessarily suffice as accurate reference models since only the time variations from the average of a seismic array are used in the inversion [16,36]. Instead, we found that using S–P travel-time residuals is a simple and relatively accurate way for correcting the reference model.

We handpicked the arrival times of P and SH waves from the recordings of the six events used in our imaging. Seismic anisotropy was found to be relatively weak in this region [37]. We thus assumed that the arrival times of SV and SH waves are equivalent. The averaged S–P differential time residuals (with respect to *iasp91*) are list in Table 1. Negative S–P residuals are observed from all the earthquakes, except for event 3, which has a less clear P-wave onset compared to the other events and also has a slightly different back azimuth. In general, S–P residuals are caused by the integrated velocity anomalies along ray paths from sources to receivers. If we assume the reference models are accurate globally, and that the power spectrum of heterogeneities in the mantle decreases rapidly with depth [38–43], then the major part of the residuals should originate in the upper mantle above the transition zone (<410 km) near the sources and the receivers. In order to estimate the residuals on the receiver side, we measured the S–P residuals from an intermediate earthquake roughly at the same azimuth of the array (event 7 in Table 1). The averaged value (−1.80 s) of the S–P residuals from this event is almost the same as the average of the other six events. We thus assume that a large part of this residual (−1.80 s) is caused by the structure above the 410-km discontinuity under the array. More importantly, we found a good correlation between the S–P residual times and the geologic provinces: a large negative S–P residual (~−2.1 s) in the Kaapvaal craton and a smaller negative one (~−1.2 s) in the Namaqua-Natal and Limpopo belts (Fig. 3A). We thus employed two 1D velocity models for the craton and mobile belts, respectively, with each producing the observed S–P residual times.

The negative S–P differential times are caused by relatively late arrival of the P wave and the relatively early arrival of the S wave, suggesting that the region is characterized by a lower P-wave velocity and a higher S-wave velocity (or a lower V_p/V_s ratio) relative to the *iasp91* model. Differences in V_p/V_s are also apparent on the regional scale; that is, the Archean Kaapvaal craton shows a larger negative S–P residual, and therefore a lower V_p/V_s ratio, than the adjacent Proterozoic mobile belts. A recent study of variations in seismic velocities of mantle peridotites at ambient (STP) conditions [14] suggests that the V_p/V_s ratio may be less sensitive to temperature (in the absence of a melt phase, Fig. 4A inset) than to the proportion of Fe and Mg in peridotite (e.g., Mg#, Fig. 4A). The smaller temperature dependence of V_p/V_s compared to composition (Mg#) is due to the fact that the $\mathrm{d}\ln(K/G)/\mathrm{d}T$ for olivine and orthopyroxene have opposite signs, where K is the adiabatic bulk modulus and G is the shear modulus. The V_p/V_s ratio decreases with increasing Mg# (~0.24%/Mg#) so that a lower V_p/V_s ratio indicates a larger Mg# (Fig. 4A). At atmospheric pressure, the increase in V_p/V_s ratio as a function of temperature is less than 0.2%/500 °C. Assuming these relationships hold at elevated pressure and that the temperature difference between the Kaapvaal craton and the Proterozoic mobile belt at upper mantle depths is <100 °C according to xenolith thermobarometry [44] the regional S–P time residuals suggest that the low V_p/V_s of the Kaapvaal cratonic mantle relative to the Proterozoic mobile belts (−0.8% to −1.2%) is due to compositional differences.

Assuming that our S–P travel-time residuals represent the integrated effects of upper mantle heterogeneities concentrated above the 410-km discontinuity, we can use the parameterizations of [14]

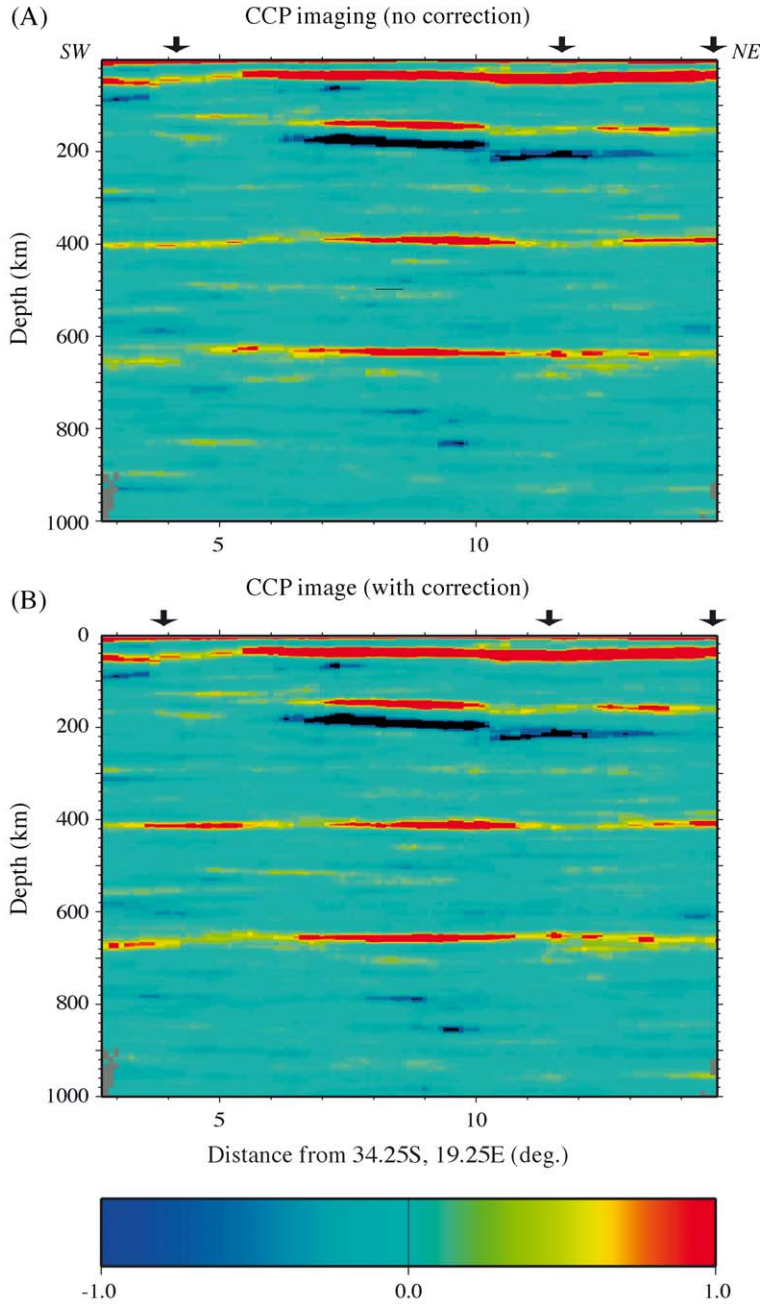

Fig. 2. (A) CCP stacked image of cross-section BB′ shown in Fig. 1. *P* to *S* converted energy is indicated by colors; hotter colors represent greater energy. Note that the Moho, the 410- and 660-km discontinuities are clearly imaged. Red and dark blue lines at ~ 100–200 km depths beneath the Kaapvaal craton are crustal reverberations. The three arrows roughly indicate the locations of Namaqua-Natal Belt, the Bushveld Complex, and the Limpopo Belt. Imaging is based on *P* to *S* conversion times calculated from the 1D velocity model, *iasp91*. (B) Same with panel (A) except a time correction is applied to account for the negative S–P residuals observed across the seismic array.

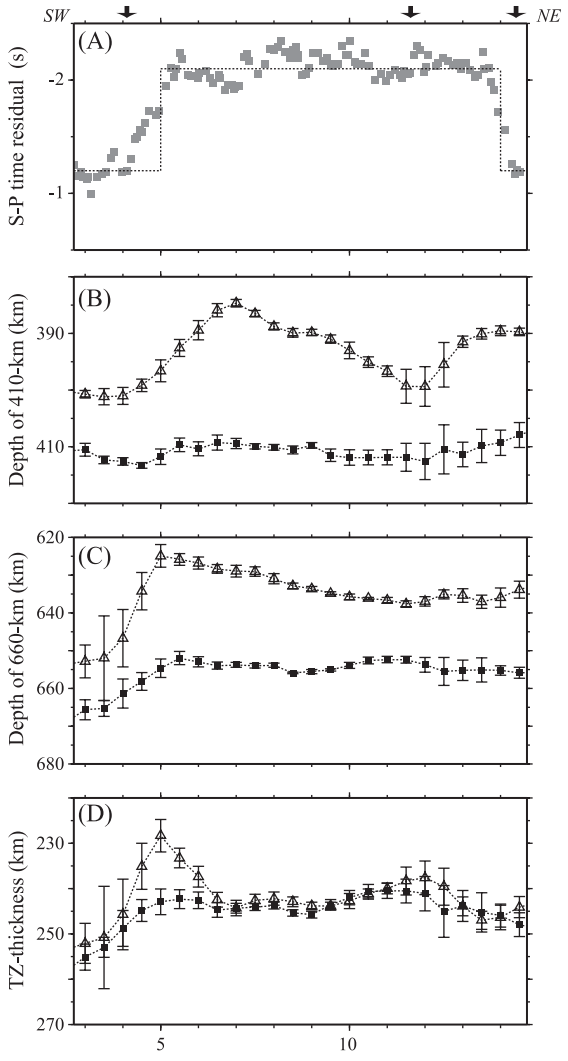

Fig. 3. S–P travel-time residuals (A) are shown with the variations of the depths of the 410-km (B), 660-km (C) discontinuities and the transition-zone thickness (D) along the line BB′ shown in Fig. 1. All the values are averaged across a 1° window. The three arrows indicate the locations of Namaqua-Natal Belt, the Bushveld Complex, and the Limpopo Belt. Dotted line in panel (A) shows the time corrections employed. Triangles and squares in panels (B), (C) and (D) indicate the measurements before and after the velocity correction, respectively. Errors are calculated using a bootstrap method [46].

and our V_p/V_s constraints to estimate Mg#. The average S–P residual time shows a difference of 0.9 s between the Kaapvaal craton and the surrounding belts. We estimate the difference in V_p/V_s ratio to be ~0.8–1.2% under the assumption that the S–P travel-time residuals are evenly distributed above the 410-km discontinuity. Based on the published value of the slope $d(V_p/V_s)/dMg\# = \sim 0.0041$ [14], we obtain a difference of ~3–5 in Mg#, which indicates that the Mg# beneath the Archean Kaapvaal craton is ~3–5 times higher than that beneath the adjacent Proterozoic terranes. While this result is consistent with xenolith observations that the Archean cratonic mantle is more depleted than the surrounding Proterozoic mantle, the inferred difference in Mg# is probably a maximum estimate for two reasons. First, our calculations do not take into account the role of garnet- and pyroxene-rich lithologies, such as eclogites. The V_p/V_s ratio of eclogites is roughly 3% higher than typical peridotites so that a 10% eclogite component would correspond to a ~0.3% increase in V_p/V_s. If eclogite lithologies are present in the Proterozoic regions as suggested by [45], the presence of 10% would reduce our estimated difference in Mg# between the Archean and Proterozoic mantles to 2–4. Our estimated Mg# differences might be further reduced given that part of the observed S–P travel-time residuals may have been introduced from crustal structure. Although it is difficult to quantify these effects precisely, our observations qualitatively indicate that the Kaapvaal tectospheric mantle is much more depleted than the mantle beneath surrounding mobile belts.

The CCP stacked image with the corrections is shown in Fig. 2B. The corrections were made by back projecting the observed S–P travel-time residuals to the ray paths above the 410-km discontinuity under the array. Compared to Fig. 2A, the image is improved in two aspects: (1) the two discontinuities are imaged at greater depths, with values closer to the global averages; (2) better images of the two discontinuities are obtained in the transition regions between the Namaqua-Natal Belt and the Kaapvaal craton. For example, the 660-km discontinuity appears as a diffuse event spread over ~50 km in the southwestern ~250 km of the uncorrected CCP image (Fig. 2A). After the travel-time correction, the 660-km appears much sharper (Fig. 2B). Both the 410- and the 660-km discontinuities are extremely well mapped in the CCP image with a simple velocity correction (Fig. 2B).

The measured depths of the two discontinuities and the transition-zone thickness are shown in Fig. 3. Errors are estimated using a bootstrap method [46].

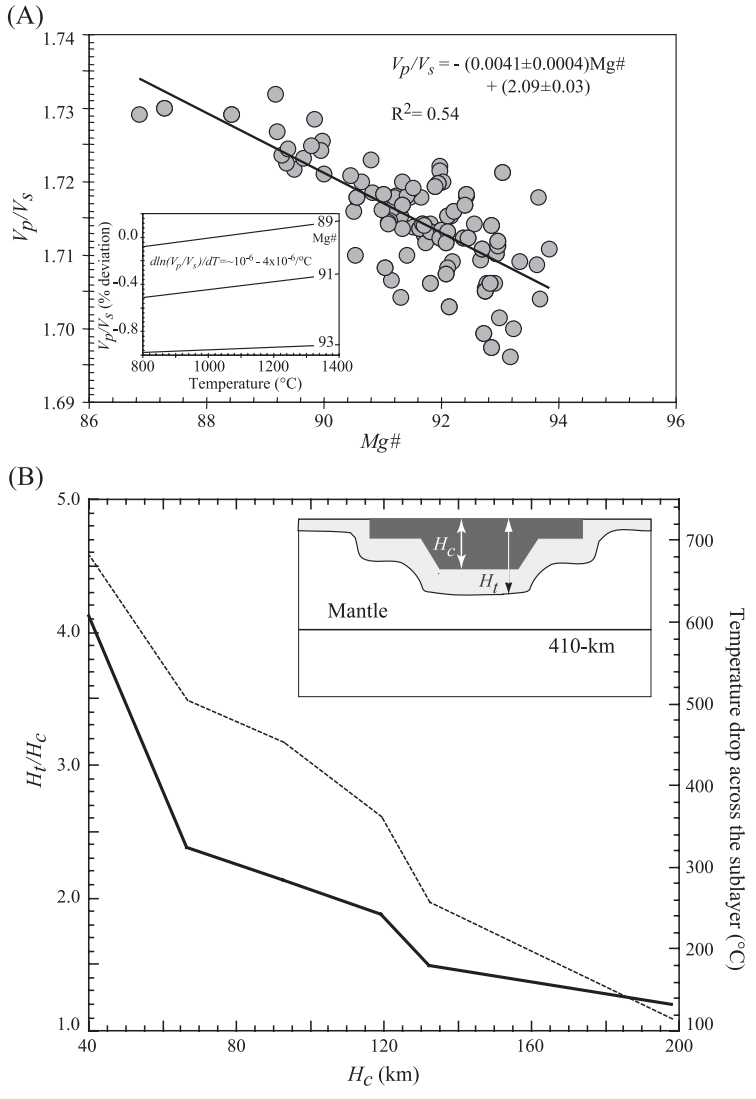

Fig. 4. (A) The V_p/V_s ratio at standard temperature and pressure (1 atm and 25 °C) conditions are plotted against bulk Mg#. Note the ratio shows a good negative correlation with Mg#. All the V_p and V_s values shown here are calculated for natural peridotite samples whose mineral chemistries and bulk compositions have been measured. Elastic moduli are based on existing experiment data. Hashin–Shritkman averaging is used in determining bulk elastic moduli. Only Garnet-facies peridotites which represent peridotite samples from greater than ~ 1.5 GPa (~ 45 km) are used. Inset shows the dependence of V_p/V_s ratio on temperature [$\delta\ln(V_p/V_s)/\delta T$] for different bulk Mg#'s. (B) The ratio of the entire thermal to CBL thickness (Solid line) and the temperature drop across the thermal sublayer (dotted line) are plotted against the thickness of the CBL. A cartoon illustrating the thermal lithosphere, which is made of a CBL and a subkeel thermal layer with a composition identical to convecting mantle, is shown in the inset. The thickness of the continental crust is fixed at 40 km.

Before the correction, large depth variations (~20–30 km) are observed for both the 410- and the 660-km discontinuities (triangles in Fig. 3B and C). After the correction, however, the two discontinuities become very flat, with depth variations less than 5 km except for a ~15-km depression in the 660-km beneath the Namaqua-Natal Belt (squares in Fig. 3B and C). Tomographic images [16] show large, low velocity anomalies at transition-zone depths beneath the Namaqua-Natal Belt. Part of the depression of the

660-km discontinuity thus may be introduced by these unmodeled velocity anomalies. Although there are some uncertainties in attributing all of the S–P travel-time residuals to receiver-side structure, the azimuthal variation of the earthquakes we examined indicates that the difference in S–P times between the craton and surrounding belts (0.9 s) must result entirely from receiver side structure at depths above the transition zone.

Our results thus agree with the observation made along the eastern margin of the North American craton [12]. Chevrot et al. [47] made a worldwide investigation of Pds by stacking receiver functions collected at a station, a method known as single-station gathering and often used when array data are not available. They showed that the transition-zone thickness appears to be normal beneath most of cratons. Our results here thus are consistent with their observations if we assume that an ordinary thick transition zone means that the two discontinuities are at normal depths and are also flat. If the 410-km discontinuity is due to a temperature-sensitive phase transition, as believed [11], then a lack of topography in the discontinuity under a region suggests that large temperature variations would not be present near the discontinuity. Therefore, a flat 410-km discontinuity underneath a cratonic region would imply that large-scale downwellings might not be forming at the base of the thick cratonic root. To explore this further, we conducted numerical simulations that model chemically distinct continents residing within the upper boundary layer of a convecting mantle [48]. Cratonic roots of variable thickness were included at the base of the continental crust. The entire chemical boundary layer (CBL, defined as continental crust plus cratonic root) was not allowed to participate in convective overturn, but continents could drift freely. We found that a thermal sublayer (bright shading, Fig. 4B inset) forms at the base of the cold CBL (dark shading, Fig. 4B inset). The thickness of the sublayer decreases rapidly with the increasing thickness of the CBL such that when the CBL thickness exceeds 160 km the entire thermal lithosphere (CBL + sublayer) becomes dominated by the CBL (Fig. 4B). When the CBL is thin, a thick sublayer forms, which can finally develop into a thermal downwelling with a scale roughly similar to the thickness of the sublayer and a temperature anomaly comparable to the temperature drop across the sublayer. Both the large temperature drop and thickness would lead to a large density anomaly that could deflect the 410-km discontinuity. When the CBL reaches a thickness of 160 km, the temperature difference across the sublayer and the sublayer thickness both become small and any downwellings that could develop are associated with small density anomalies. Thus, a flat 410-km discontinuity, which suggests no large-scale downwellings, gives us a constraint on the minimum thickness, $\sim$160 km, of the CBL. On the other hand, a flat 410-km discontinuity also means that the mean thickness of sublayer (independent of dynamic downwellings) must be confined above the discontinuity, placing an upper bound on the thickness of the CBL. If we use $H_t/H_c = 1.1$ (Fig. 4B), then we obtain the maximum thickness, H_c, to be $\sim$370 km. We thus conclude that the thickness of the CBL beneath Kaapvaal craton must be within 160–370 km.

4. Conclusions

In summary, we have shown that seismic observations on V_p/V_s structure and the topography of the 410-km discontinuity can be used to infer the composition and the depth of cratonic lithospheric mantle. These observations provide evidence independent of xenolith studies that continental keels are indeed made of highly depleted peridotites. The combination of xenolith studies and V_p/V_s seismic studies may in the future provide unprecedented constraints on the composition of the uppermost mantle. Because xenolith studies are inherently limited by sampling bias in terms of time and space, the ability to estimate composition from seismic studies should enhance our ability to map out major compositional heterogeneities in the upper mantle, particularly in regions where xenolith samples do not exist. Finally, the combination of seismic observations with geodynamical modeling allows us place limits on the thickness of continental lithosphere.

Acknowledgements

We thank all the people involved in the Kaapvaal project. We also thank M. Fouch for sharing us with

his tomographic models, R. van der Hilst, S. Chevrot and K. Dueker for their constructive comments on the submitted manuscript. This work was supported by the Department of Earth Science, Rice University (Lee, Niu), NSF CMG grants EAR-0222270 (Levander) and EAR-0001029 (Cooper and Lenardic), and Carnegie Institution of Washington (James). *[RH]*

References

[1] T.H. Jordan, The continental tectosphere, Rev. Geophys. Space Phys. 13 (1975) 1–12.
[2] T.H. Jordan, Structure and formation of the continental tectosphere, in: M.A. Menzies, K.G. Cox (Eds.), J. Petrology, Special Lithosphere Issue, Trans. R. Soc. London, London, 1988, pp. 11–37.
[3] A.L. Lerner-Lam, T.H. Jordan, How thick are the continents? J. Geophys. Res. 92 (1987) 14007–14026.
[4] S.P. Grand, Mantle shear structure beneath the Americas and surrounding oceans, J. Geophys. Res. 99 (1994) 11591–11621.
[5] J. Polet, D.L. Anderson, Depth extent of cratons as inferred from tomographic studies, Geology 3 (1995) 205–208.
[6] C. Jaupart, J.C. Mareschal, L. Guillou-Frottier, A. Davaille, Heat flow and thickness of the lithosphere in the Canadian Shield, J. Geophys. Res. 103 (1998) 15269–15286.
[7] R. Rudnick, W. McDonough, R. O'Connell, Thermal structure, thickness and composition of continental lithosphere, Chem. Geol. 145 (1998) 395–411.
[8] F.J. Simons, A. Zielhuis, R.D. Van der Hilst, The deep structure of the Australian continent inferred from surface wave tomography, Lithos 48 (1999) 17–43.
[9] F.J. Simons, R.D. Van der Hilst, Anisotropic structure and deformation of the Australian lithosphere, Earth Planet. Sci. Lett. 211 (2003) 271–286.
[10] Y. Gung, M. Panning, B. Romanowicz, Global anisotropy and the thickness of continents, Nature 422 (2003) 707–711.
[11] T. Katsura, E. Ito, The system Mg_2SiO_4–Fe_2SiO_4 at high pressures and temperatures: precise determination of stabilities of olivine, modified spinel, and spinel, J. Geophys. Res. 94 (1989) 15663–15670.
[12] A. Li, K.M. Fischer, M.E. Wysession, T.J. Clarke, Mantle discontinuities and temperature under the North America, Nature 395 (1998) 160–163.
[13] F.R. Boyd, Compositional distinction between oceanic and cratonic lithosphere, Earth Planet. Sci. Lett. 96 (1989) 15–26.
[14] C.-T.A. Lee, Compositional variation of density and seismic velocities in natural peridotites at STP conditions: implications for seismic imaging of compositional heterogeneities in the upper mantle, J. Geophys. Res. 108 (2003) 2441 (doi 10.1029/2003JB002413).
[15] M.J. de Wit, C. Roering, R.J. Hart, R.A. Armstrong, C.E.J. de Ronde, R.W. Green, M. Tredoux, E. Peberdy, R.A. Hart, Formation of an Archean continent, Nature 357 (1992) 553–562.
[16] D.E. James, M.J. Fouch, J.C. VanDecar, S. van der Lee, Kaapvaal Seismic Group, Tectospheric structure beneath southern Africa, Geophys. Res. Lett. 28 (2001) 2485–2488.
[17] T.K. Nguuri, J. Gore, D.E. James, S.J. Webb, C. Wright, T.G. Zengeni, O. Gwavana, J.A. Snoke, Kaapvaal Seismic Group, Crustal structure beneath southern Africa and its implications for the formation and evolution of the Kaapvaal and Zimbabwe cratons, Geophys. Res. Lett. 28 (2001) 2501–2504.
[18] F. Niu, D.E. James, Fine structure of the lowermost crust beneath the Kaapvaal craton and its implications for crustal formation and evolution, Earth Planet. Sci. Lett. 200 (2002) 121–130.
[19] D.E. James, F. Niu, J. Rokosky, Crustal structure of the Kaapvaal craton and its significance for early crustal evolution, Lithos 71 (2003) 413–429.
[20] J. Stankiewicz, S. Chevrot, R.D. Van der Hilst, M.J. De Wit, Crustal thickness, discontinuity depth, and upper mantle structure beneath southern Africa: constraints from body wave conversions, Phys. Earth Planet. Inter. 130 (2002) 235–252.
[21] R.W. Carlson, T.L. Grove, M.J. de Wit, J.J. Gurney, Program to study the crust and mantle of the Archean craton in southern Africa, EOS Trans. AGU 77 (1996) 273–277.
[22] C.A. Langston, Structure under Mountain Rainer, Washington, inferred from teleseismic body waves, J. Geophys. Res. 84 (1979) 4749–4762.
[23] T.J. Owens, G. Zandt, S.R. Taylor, Seismic evidence for an ancient rift beneath the Cumberland plateau, Tennessee: a detailed analysis of broadband teleseismic P waveforms, J. Geophys. Res. 89 (1984) 7783–7795.
[24] L.P. Vinnik, Detection of waves converted from P to SV in the mantle, Phys. Earth Planet. Inter. 15 (1977) 39–45.
[25] F. Niu, H. Kawakatsu, Complex structure of the mantle discontinuities at the tip of the subducting slab beneath the northeast China: a preliminary investigation of broadband receiver functions, J. Phys. Earth 44 (1996) 701–711.
[26] R.W. Clayton, R.A. Wiggins, Source shape estimation and deconvolution of teleseismic body waves, Geophys. J. R. Astron. Soc. 47 (1976) 151–177.
[27] C.J. Ammon, The isolation of receiver effects from teleseismic P waveforms, Bull. Seismol. Soc. Am. 81 (1991) 2504–2510.
[28] K.G. Dueker, A.F. Sheehan, Mantle discontinuity structure from midpoint stacks of converted P and S waves across the Yellowstone hotspot track, J. Geophys. Res. 102 (1997) 8313–8328.
[29] F. Niu, S.C. Solomon, P.G. Silver, D. Suetsugu, H. Inoue, Mantle transition-zone structure beneath the South Pacific Superswell and evidence for a mantle plume underlying the Society hotspot, Earth Planet. Sci. Lett. 198 (2002) 371–380.
[30] B.L.N. Kennett, E.R. Engdahl, Travel times for global earthquake location and phase identification, Geophys. J. Int. 105 (1991) 429–465.
[31] K.J. Muirhead, Eliminating false alarms when detecting seismic events automatically, Nature 217 (1968) 533–534.

[32] E.R. Kanasewich, Time Sequence Analysis in Geophysics, University of Alberta Press, Edmonton, AB, 1973 (364 pp.).
[33] S.S. Gao, P.G. Silver, K.H. Liu, Kaapvaal Seismic Group, Mantle discontinuities beneath southern Africa, Geophys. Res. Lett. 29(10.1029/2001GL013834).
[34] M.P. Flanagan, P.M. Shearer, Global mapping of the topography on the transition zone velocity discontinuities by stacking SS precursors, J. Geophys. Res. 103 (1998) 2673–2692.
[35] Y. Gu, A.M. Dziwonski, C.B. Agee, Global de-correlation of the topography of transition zone discontinuities, Earth Planet. Sci. Lett. 157 (2004) 57–67.
[36] J.-J. Leveque, F. Masson, From ACH tomographic models to absolute velocity models, Geophys. J. Int. 137 (1999) 621–629.
[37] P.G. Silver, S.S. Gao, K.H. Liu, Kaapvaal Seismic Group, Tectospheric structure beneath southern Africa, Geophys. Res. Lett. 28 (2001) 2493–2496.
[38] A.M. Dziewonski, Mapping the lower mantle: determination of lateral heterogeneity in P velocity up to degree and order 6, J. Geophys. Res. 89 (1984) 5929–5952.
[39] J.H. Woodhouse, A.M. Dziewonski, Mapping the upper mantle: three-dimensional modeling of Earth structure by inversion of seismic waveforms, J. Geophys. Res. 89 (1984) 5953–5986.
[40] W. Su, R.L. Woodward, A.M. Dziewonski, Degree 12 model of shear velocity heterogeneity in the mantle, J. Geophys. Res. 99 (1994) 6945–6980.
[41] X.-D. Li, B. Romanowicz, Global mantle shear-velocity model using nonlinear asymptotic coupling theory, J. Geophys. Res. 101 (1996) 22245–22272.
[42] R.D. van der Hilst, S. Widiyantoro, E.R. Engdahl, Evidence for deep mantle circulation from global tomography, Nature 386 (1997) 578–584.
[43] Y. Fukao, S. Widiyantoro, M. Obayashi, Stagnant slabs in the upper and lower mantle transition zone, Geophys. Rev. 39 (2001) 291–323.
[44] D.E. James, F.R. Boyd, D. Schutt, D.R. Bell, R.W. Carlson, Xenolith constraints on seismic velocities in the upper mantle beneath southern Africa, Geochem. Geophys. Geosyst. 5 2004 (doi 10.1029/2003GC000551).
[45] S.B. Shirey, J.W. Harris, S.H. Richardson, M.J. Fouch, D.E. James, P. Cartigny, P. Deines, F. Viljoen, Diamond genesis, seismic structure, and evolution of the Kaapvaal–Zimbabwe Craton, Science 297 (2002) 1683–1686.
[46] B. Efron, R. Tibshirani, Bootstrap methods for standard errors, confidence intervals, and other measures of statistical accuracy, Stat. Sci. 1 (1986) 54–75.
[47] S. Chevrot, L. Vinnik, J.P. Montagner, Global scale analysis of the mantle Pds phases, J. Geophys. Res. 104 (1999) 20, 203–20219.
[48] C.M. Cooper, A. Lenardic, L. Mores, The thermal structure of stable continental lithosphere within a dynamic mantle, Earth Planet. Sci. Lett. 222 (2004) 807–817.